Peer-reviewed version available at *ISPRS Int. J. Geo-Inf.* **2017**, *6*, 401; doi:10.3390/ijgi6120401

Article

A remote sensing approach to subsidence and vegetation degradation in a reclaimed mine area

Rajchandar Padmanaban[1*], Avit K. Bhowmik[2], and Pedro Cabral[1]

[1] NOVA IMS, Universidade Nova de Lisboa, Campus de Campolide, 1070-312 Lisbon, Portugal
[2] Stockholm Resilience Centre, Stockholm University, Kraftriket 2B, SE-104 05 Stockholm, Sweden
* Correspondence: rajchandar07@gmail.com

Abstract: Mining for resources extraction may lead to several geological and associated environmental changes due to ground movements, collision with mining cavities and deformation of aquifers. Geological changes may continue in a reclaimed mine area, and the deformed aquifers may entail a breakdown of substrates and an increase in ground water tables, which may cause surface area inundation. Consequently, a reclaimed mine area may experience surface area collapse, i.e. subsidence, and degradation of vegetation health. Thus, monitoring short-term landscape dynamics in a reclaimed mine area may provide important information on the long-term geological and environmental impacts of mining activities. We studied landscape dynamics in Kirchheller Heide, Germany, which experienced extensive soil movement due to longwall mining without stowing, using Landsat imageries between 2013 and 2016. A Random Forest image classification technique was applied to analyse land-use and land-cover dynamics and the growth of wetland areas was assessed using a Spectral Mixture Analysis (SMA). We also analyzed the changes in vegetation health using a Normalized Difference Vegetation Index (NDVI). We observed a 19.9% growth of wetland area within the four years with 87.2% of growth in the coverage of two major waterbodies in the reclaimed mine area. NDVI values indicate that 66.5% of the vegetation of the study area was degraded due to changes in ground water tables and surface flooding. Our results inform environmental management and mining reclamation authorities about the subsidence spots and priority mitigation areas from land surface and vegetation degradation in Kirchheller Heide.

Keywords: Mining; Mine reclamation; Land cover change; Vegetation health; NDVI Post-mining; SMA; Random forest classification; Remote Sensing

1. Introduction

Mining is an important source of raw materials and minerals, e.g. metals, salt and coal, for industrial and domestic usage [1,2]. Countries in the European Union produce about 7% of the industrial and domestic commodities from mine extracted resources [2]. Mining industries also play a vital role in global to regional economies, e.g. in energy production and fuel supply [1].

Mining activities may lead to several geological changes, i.e. ground movements, collision with mining cavities and deformation of aquifers (Figure 1). These changes may constitute an increase in the groundwater table, and thus a slow sinking of subsurface soils and an unexpected collapse, i.e. subsidence [2]. The extraction processes and machines used to access mine galleries may produce irreversible damages in soil cohesion and eventually compress soil substrates [3,4]. Consequently, groundwater may intrude the surface level, form new waterbodies and cause inundation. This, in turn, leads to several adverse environmental impacts, such as vegetation degradation, soil erosion, flooding, sinkhole formation, and soil and water contamination [5–8] as well as to damages of infrastructures [9]. The geological changes and associated environmental impacts may continue even after reclamations if mines are not properly backfilled [10-12].

Regular landscape management and monitoring at the surface level are crucial for the prevention of subsidence and development of early warning systems in a reclaimed mine area (Figure 1). These are also vital for environmental protection as well as for mitigation of the aftermaths from mining activities [2]. Particularly, monitoring short-term landscape dynamics and changes in

Peer-reviewed version available at ISPRS Int. J. Geo-Inf. 2017, 6, 401; doi:10.3390/ijgi6120401

the extent of waterbodies may provide important information about long-term geological changes and associated effects on the environment [8,9]. In addition, changes in the health of vegetation is an important indicator for assessing the geological changes in an active and reclaimed mine area [13,14]. Health of vegetation may surrogate ecological health as well as growth of water bodies and plant stress [1,8,13].

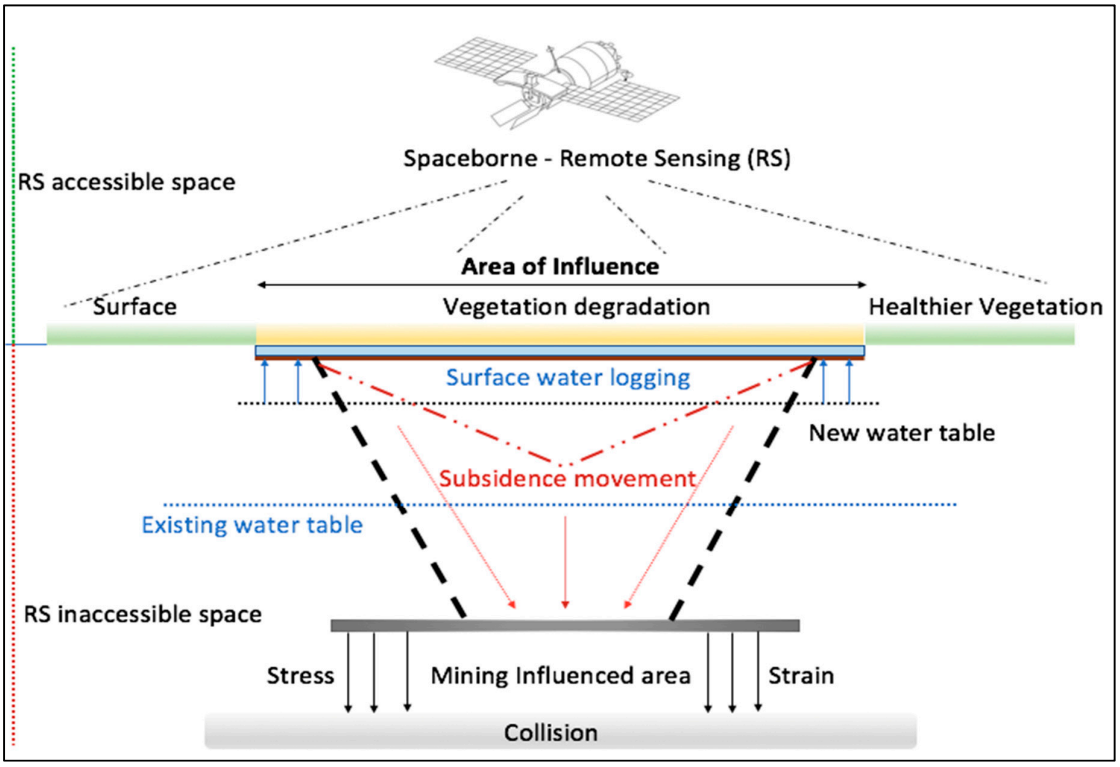

Figure 1. Inundation and subsidence through geological changes in a mining affected area. The changes observed in the surface level using remote sensing (RS) may indicate the geological changes at the subsurface level. The figure is created according to the description of subsidence in Brunn et al. (2002) [4].

Remote Sensing (RS) techniques and Geographic Information Systems (GIS) have shown clear advantages over conventional field monitoring and laboratory measurements for assessing long-to short-term landscape dynamics [15–17]. Particularly for large areas, where surveying using Global Positioning System (GPS) and ground levelling are time consuming, expensive and labor-intensive, RS and GIS provide prompt and efficient information on geological changes and subsidence [8]. These techniques are also useful for detecting changes in vegetation health and cover, and flood dynamics through land-use and landcover maps [18]. Multispectral satellite images allow for detecting gradual as well as abrupt changes in landscapes [19]. However, besides widespread application in monitoring general landscape dynamics, the application of RS and GIS in monitoring and assessing mining effects on landscapes and environment, and in associated geological changes and vegetation health dynamics is limited [4,10,20]. Although high resolution Light Amplification by Stimulated Emission of Radiation (LASER), Interferometric Synthetic Aperture Radar (InSAR) and Light Detection and Ranging (LIDAR) mapping have been sparsely applied in small areas, environmental impacts in large mine reclamation areas have rarely been investigated using RS and GIS techniques [21-26].

This study aims to identify the subsidence zones and vegetation degradation in a reclaimed mine area through the analyses of short-term landscape dynamics using RS and GIS techniques. The specific objectives were:

(1) To examine the short-term, i.e. during 4 years, land-use and landcover (LULC) dynamics in the reclaimed mine area;

(2) To quantify the emergence and growth of wetlands in the mining influenced area and thus to identify potential subsidence spots, i.e. spots exhibiting abrupt growth of waterbodies; and

(3) To examine the vegetation health dynamics as a surrogate of the ground water table fluctuation and ecological stress.

2. Study area

The study area "Kirchheller Heide" (in English "Kirchhellen Heath"), is located in western Germany, between the towns of Bottrop and Huxe in the North, Oberhausen in the South, Gladbeck in the East and Dinslanken in the West (Figure 2). The mining reclamation area lies between 51° 34′ 53″ N and 6° 51′ 50″ E and covers an area of about 5,774 ha. This site is one of the recreation areas for 7.5 million residents of the Kirchheller Heide and Ruhr district [2].

The area was a major industrial region dominated by 229 coal and steel mines from the second half of the 19th to the end of the 20th century, which produced approximately 400,000 tons of coal per year [2]. The coal was extracted from this area from depths up to 1500m using the longwall mining method [2]. This mining method creates cavities in the ground and rock formation, which may result in surface subsidence and changes in the ground water table [20]. Moreover, the area was not properly backfilled when reclaimed [1]. Hence, this area was chosen to study potential occurrence of subsidence and inundation caused by mining activities [2].

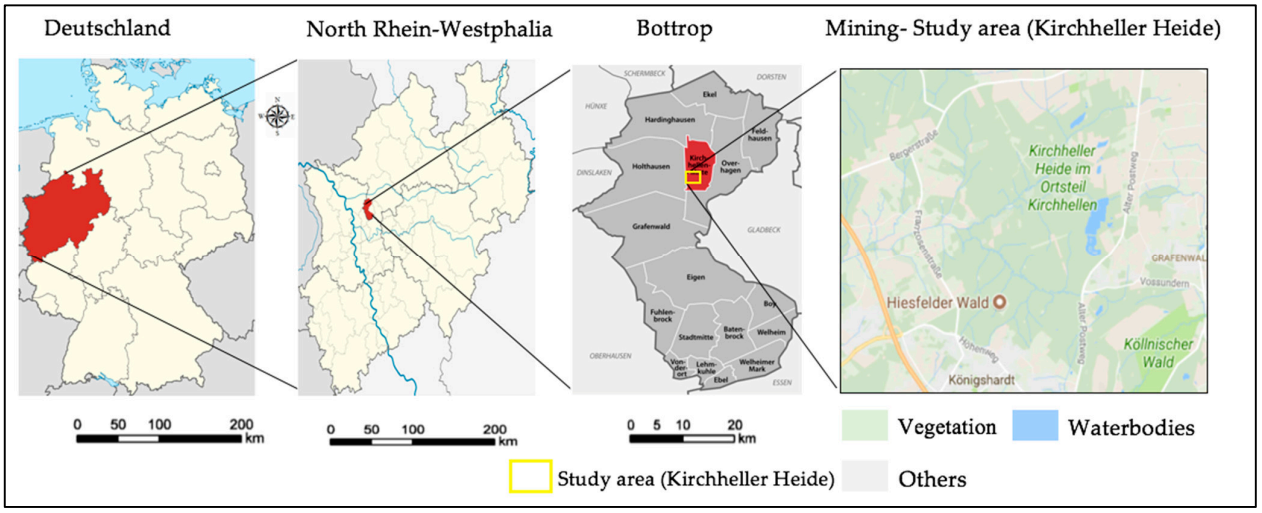

Figure 2. Location of Kirchheller Heide and mining area. The maps were created using [map source: google maps]

3. Materials and methods

3.1. Satellite data

We used four Landsat Enhanced Thematic Mapper plus (ETM+) imageries covering years 2013-2016 with 30m spatial resolution [27-30]. To be consistent with seasonal variations and vegetation health analysis, we selected images covering frost-free growing season of Germany. This season starts in May (Spring) and ends in September (Fall) [4]. To be further consistent with vegetation proportion, we selected images of July (growing season), which recorded consistent precipitation level varying between 28.2 and 34.4 liter per m² during 2013-2016 [31]. Landsat ETM+ data were freely downloaded from the United States Geological Survey (USGS) gateway [29,30].

3.2. Image processing

We followed a four-step procedure for investigating the landscape dynamics and vegetation health in Kirchheller Heide (see Figure 3). First, the satellite images were ortho-rectified and geo-corrected using the available "geoshift" and "georef" functions of the "Landsat" package in R studio [32]. Then, we geo-referenced the images using Universal Transverse Mercator (UTM) coordinate system [27]. The ETM+ images were cropped to the study area using a 10km buffer around the mining area using ERDAS Imagine (version 8.7) [30-33]. To enhance the separability of mining area from other land-use and landcover types, we applied the Tasseled Cap correction for each imagery based on digital numbers (DN) [32-34].

To distribute and store the Landsat images in a common radiometric scale, we converted digital number (DN) integer values (0-255) to at-satellite radiance values using the available parameters in the ETM+ metadata (radiometric calibration), i.e. Top-of-Atmosphere (TOA) radiance [35-40]. We also applied atmospheric correction to overcome the mismatch between surface reflectance and at-sensor reflectance. For the purpose, the cloud, snow, aerosol and cirrus were first identified and classified, and then were removed. Then, the atmospheric correction was applied and the atmospheric differences caused by various Pseudo-Invariant Features (PIF) were overcome. The radiometric and atmospheric corrections were conducted employing Landsat and RStool packages available in the R library [41-45].

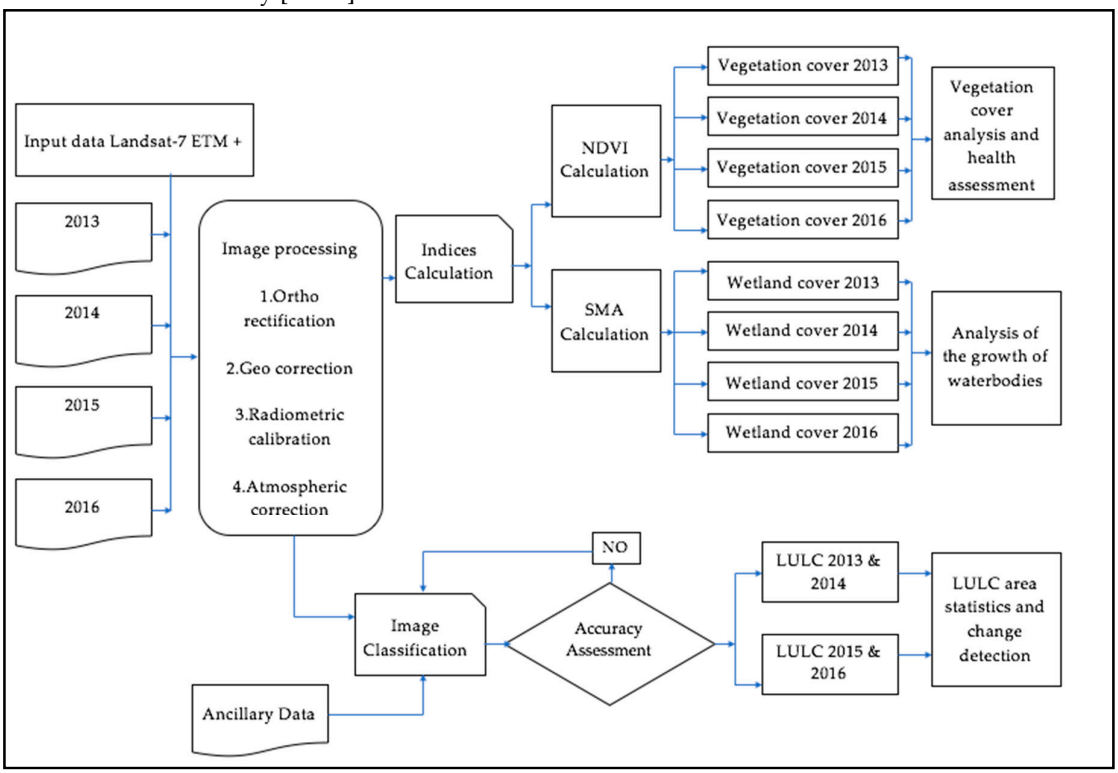

Figure 3. Methodology for the analysis of landscape dynamics and vegetation health [NDVI: Normalized Difference Vegetation Index, ETM: Enhanced Thematic Mapper, SMA: Spectral Mixture Analysis and LULC: Land-use and Land cover].

3.3. Land-use and landcover classification and accuracy assessment

We analysed the overall surface level landscape dynamics over the four years using an unsupervised image classification technique. The images were classified for 2013, 2014, 2015 and 2016 into five land-use and landcover (LULC) classes (Table 1). We applied a Random Forest (RF) classification technique that optimizes the proximities among data points [41-43]. The RF classification algorithm used the following steps:

- Draw n-tree bootstrap model from the satellite imageries;

Peer-reviewed version available at ISPRS Int. J. Geo-Inf. 2017, 6, 401; doi:10.3390/ijgi6120401

- For each bootstrap model: grow unpruned classification according to the DN values;
- Generate N number of polygons according to the DN values;
- Choose five classification land-use classes;
- Display land-use classification.

The LULC classification was performed in R [41] using Classes and Methods for Spatial Data (Sp), Raster Geospatial Data Abstraction Library (Rgdal), Raster, and Random forests packages [42-45].

Table 1. Description of Landuse and Landcover (LULC) classes

No	LULC Classes	Land Uses Involved in the Class
1	Settlement	Urban built-up and roads
2	Dense vegetation	Forests, gardens and shrubs
2	Waterbodies	Rivers, lakes, ponds, open water and streams
3	Agriculture	Farms and Agriculture parcels
4	Bare land	Non-irrigated properties and Dry lands

The accuracy of image classification was evaluated by comparing the classified LULC maps with reference Google Earth images from 2013 – 2016 of the study area obtained from Google Earth Engine (GEE) platform [27]. We produced a set of 75 random points and extracted those values for four different study periods. Then, the selected random point values were identified from GEE and compared to the LULC maps. We used the kappa coefficient to quantify the accuracy of the classified images using ERDAS Imagine (version 8.7) [38,39]. The user and producer accuracies were also calculated through a confusion matrix [16]. A kappa coefficient of more than 0.8 indicates a satisfactory accuracy of classified images, i.e. classified images are analogous to the reference data [46-50].

3.4 Wetland coverage and surface flooding

The dynamics of wetland coverage as well as the extent of surface flooding were assessed to identify potential subsidence zones. We applied a SMA on the Landsat imageries to track the changes in wetland coverage and identify the emergence of waterbodies [50,22]. SMA delivers pixel estimates for water extent delineated from other landcover pixels based on available radiometric data in imageries [51] (equations 1 & 2).

$$DN_i \sum_j F_j \, DN_{i,j} + r_i \qquad (1)$$

$$\sum_j F_j = 1 \qquad (2)$$

Where, DN_i is the measured value of a mixed pixel in band i; DN_j is the measured value of each endmember (wetland pixel); F_j is the fraction of each endmember; r is the root mean square (rms) residual that accounts for the difference between the observed and modeled values [51]. Thus, waterbodies and their extent were delineated from other landcover classes for each year during 2013-

2016. We calculated the total and individual area coverage of waterbodies in each year as well as identified if any waterbody emerged. SMA calculation and changes in waterbodies were analysed using R packages SP, Rgdal, Raster and Raster Time Series Analysis (rts) [41-43].

3.5. Vegetation health and coverage

We calculated the Normalized Difference Vegetation Index (NDVI) for the quantification of vegetation health during 2013-2016 using equation 3 [40-43]:

$$NDVI = (NIR - Red)/(NIR + Red) \quad (3)$$

Where, NIR = Near Infrared Band value and R = Red Band value recorded by the Landsat ETM+ imageries [44]. The photosynthesis is the main function of plants, which is directly associated with electromagnetic energy [59,60]. The spectrum of visible region strongly absorbed by green vegetation and reflects in the NIR region [43]. NDVI performed the NIR and R band-ratio to describe the relative density and health of vegetation greenness. Thus, we integrated plant ecological functions with available radiometric data of mining area associated with the principles of electromagnetic spectrum.

NDVI values ranged from -1 to +1 [45,46]. In general, highly productive healthy vegetation exhibits high NDVI values (close to +1), e.g. forests exhibit values ranging from 0.6 to 0.8 [49], whereas lowly productive vegetation exhibits NDVI values close to 0, e.g. shrubs and grasslands exhibit values between 0.2 and 0.3 [58,60]. NDVI also identifies values close to -1 as damaged vegetation, i.e. usually water, and the values below 0.1 as degraded vegetation, i.e. barren areas such as sand, rock and snow.

We classified the obtained NDVI values into 10 raster zones based on natural breaks to distinguish among different stages of vegetation health and coverage, i.e. value ranges 0.42-1, 0.08-0.42 and -1-0.08 indicated healthy (high productivity and dense canopies), unhealthy (degraded and low productivity) and damaged vegetation, respectively. We calculated the changes in the area coverage of each raster zone during 2013-2016 and thus quantified the dynamics in vegetation health and coverage. NDVI calculation and changes in vegetation health were analysed using R packages SP, Rgdal, Raster and rts [41-43].

4. Results and discussion

4.1. Landscape dynamics in Kirchheller Heide during 2013-2016

Figure 4 displays the LULC maps of Kirchheller Heide mining area obtained for the different time periods (July 2013, 2014, 2015 and 2016) using RF classification in R programming. We obtained an overall accuracy value of more than 85% for the classified LULC maps of all years with kappa coefficient values of more than 0.84 (Table 2). These values indicate the satisfactory accuracy of the classified LULC maps.

The classified LULC maps exhibit a 19.9% increase in the coverage of waterbodies between 2013 and 2016 with an annual growth rate of 6.5% (Table 3, Figure 4). This increase in the coverage of waterbodies was associated with a 5.43% decrease in the coverage of dense vegetation and 25.6% increase in the bare land area (Table 3, Figure 4). The coverage of agricultural land also exhibited a 3.2% decrease whereas the settlement coverage increased by 5.45%. The increase in the coverage of waterbodies may relate to the subsidence and changes in ground water table in the surface level [2,3]. This subsidence may have led to collision with non-stowed mining cavities, groundwater intrusion and caused surface flooding which, in turn, affected and caused the decrease in the coverage of dense vegetation and agricultural lands. These results are in line with [1], who showed the relation between surface landscape dynamics and subsurface geological changes. The observed increase in the coverage of bare land may also indicate the vegetation damage caused by the subsidence and surface flooding [3,4].

Preprints (www.preprints.org) | NOT PEER-REVIEWED | Posted: 2 November 2017 doi:10.20944/preprints201711.0019.v1

Peer-reviewed version available at ISPRS Int. J. Geo-Inf. 2017, 6, 401; doi:10.3390/ijgi6120401

Table 2. Summary of the confusion matrix for the classified images of 2013-2016.

LULC classes	2013		2014		2015		2016	
	Producer Accuracy	User Accuracy	Producer Accuracy	User Accuracy	Producer Accuracy	User Accuracy	Producer Accuracy	User Accuracy
Settlement	87.02	82.21	86.01	82.12	88.22	79.71	92.02	88.19
Dense Vegetation	83.05	83.85	82.14	85.34	81.76	81.96	83.14	87.02
Agriculture land	86.78	91.76	83.21	94.21	83.45	92.12	88.46	96.75
Water bodies	86.95	91.35	81.11	89.55	87.65	88.76	82.11	85.88
Bare land	91.21	84.12	88.54	79.32	89.31	83.66	81.43	83.23
Kappa	0.87		0.84		0.86		0.85	

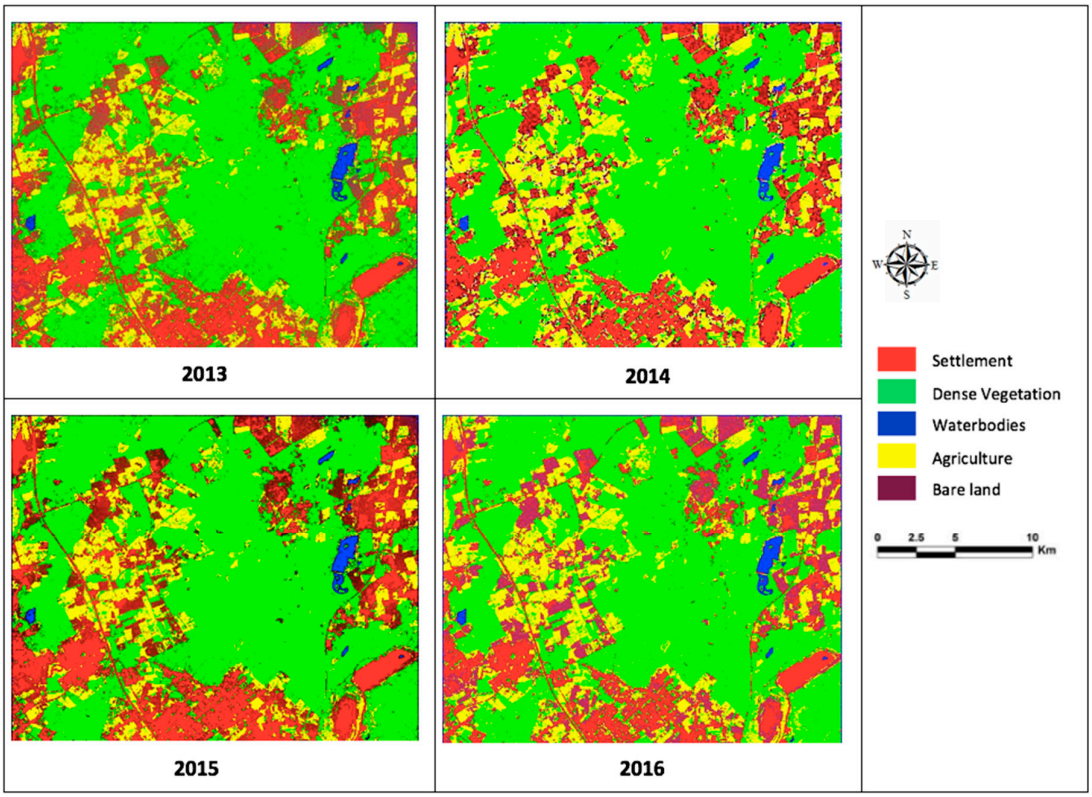

Figure 4. Classified land-use and landcover (LULC) maps of Kirchheller Heide in July 2013, 2014, 2015 and 2016.

Table 3. Comparison of the land-use and land cover (LULC) types during 2013-2016.

Area in hectare

Preprints (www.preprints.org) | NOT PEER-REVIEWED | Posted: 2 November 2017 doi:10.20944/preprints201711.0019.v1

Peer-reviewed version available at ISPRS Int. J. Geo-Inf. 2017, 6, 401; doi:10.3390/ijgi6120401

LULC classes	2013	2014	2015	2016	Differences (ha) 2013 - 2016	Differences (%) 2013 - 2016
Settlement	1270.3	1303.9	1324.7	1339.6	69.3	5.45
Dense vegetation	3077.7	3027.4	2972.1	2910.3	-167.4	-5.43
Waterbodies	28.87	30.77	32.37	34.64	5.77	19.9
Agriculture	923.91	915.50	902.31	895.03	-28.88	-3.12
Bare land	473.50	502.71	574.80	594.76	121.26	25.6

4.2. Emergence and growth of waterbodies

The SMA did not identify any emergence of waterbodies in Kirchheller Heide during 2013-2016 (Figure 5a). However, we observed an abrupt growth (5.77ha) in the coverage of two waterbodies within the four years (Figure 5a). The increase in the coverage of these two waterbodies (waterbody A and B) accounted for 87.2% of the total growth the coverage of waterbodies in Kirchheller Heide with an annual growth rate of 29% (Figure 5b and 5c). The waterbody A and B exhibited a 67% and 90% growth, respectively, in their coverage during 2013-2016 (Figure 5c). Hence, the locations of waterbodies A and B may have been the potential subsidence spots that led to surface sink, collapse and groundwater intrusion entailing an increase in the coverage of those waterbodies [2,3].

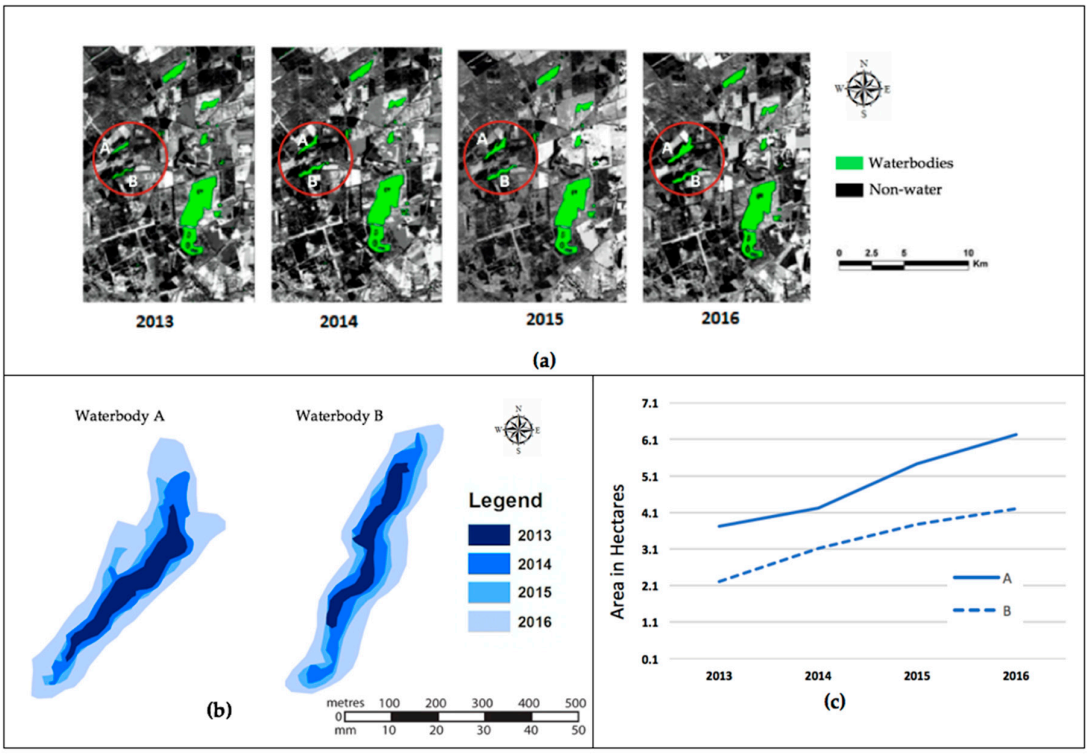

Figure 5. Changes in the extent and coverage of waterbodies in Kirchheller Heide during 2013-2016. (a) The location of waterbodies (A and B) in the red circle indicate the waterbodies with the highest (87.2%) growth and potential subsidence spots, (b) the dynamics of the extent of waterbodies A and

B during the years 2013-2016 and (c) the changes in the area coverage of waterbodies A and B during 2013-2016.

4.3. Vegetation health

We observed a substantial decrease in the area coverage of healthy vegetation, which was associated with an increase in the area coverage of unhealthy and damaged vegetation (Figure 6, Table 4). The central mining area experienced the highest decrease in NDVI values between 2013 and 2016, i.e. the average NDVI values decreased from 0.61 to 0.29 (Figure 6). A total 58.5% damage in the vegetation mostly occurred in the neighbourhood of waterbodies and along the water courses (Figure 6, Table 4). Overall, the total area coverage under healthy vegetation decreased from 56.5% to 28.3% with an annual rate of 9.5%, whereas the area coverage under unhealthy and damaged vegetation increased from 14% to 76% with an annual rate of 15.5% between 2013 and 2016 (Table 4).

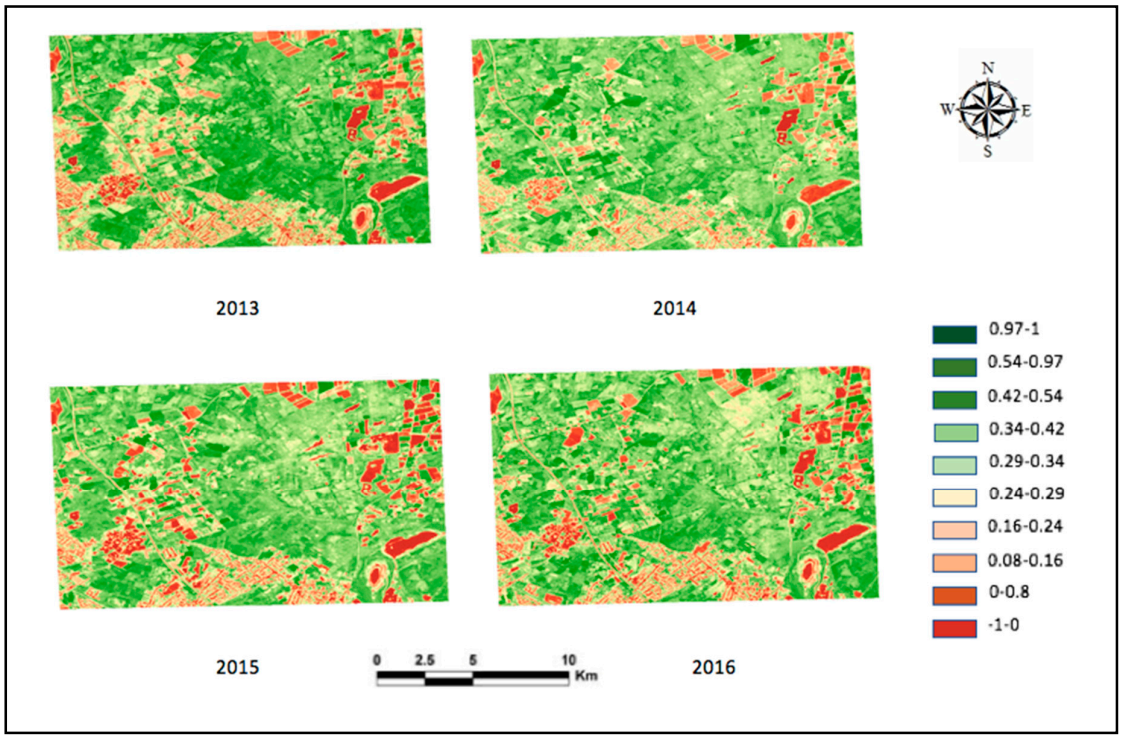

Figure 6. NDVI map of the Kirchheller Heide mining area in July 2013, 2014, 2015 and 2016. value ranges 0.42-1, 0.08-0.42 and -1-0.08 indicated healthy, unhealthy and damaged vegetation, respectively

Our results indicate an overall degradation of vegetation health with substantial damage of vegetation along the water course in Kirchheller Heide (Figure 6, Table 4). This damage was entailed by the increase in the groundwater table and consequent intrusion into the surface level (Figure 6) [3]. Increase in the groundwater table led to surface flooding as well as to soil erosion, which directly influenced the vegetation health as observed in the extent of NDVI values (Figure 6) [1,2].

Table 4. Vegetation health changes between 2013 - 2014, 2014 -2015, and 2015 - 2016. Value ranges 0.42-1, 0.08-0.42 and -1-0.08 indicated healthy (Green), unhealthy (Yellow) and damaged vegetation (Red), respectively.

Preprints (www.preprints.org) | NOT PEER-REVIEWED | Posted: 2 November 2017 doi:10.20944/preprints201711.0019.v1

Peer-reviewed version available at ISPRS Int. J. Geo-Inf. 2017, 6, 401; doi:10.3390/ijgi6120401

NDVI Values	NDVI values & area changes in % (ha) from 2013 to 2014		NDVI values & area changes in % (ha) from 2014 to 2015		NDVI values & area changes in % (ha) from 2015 to 2016	
0.97-1	Decreased by 6%	(27.36)	Decreased by 8%	(36.48)	Decreased by 12%	(54.72)
0.54-0.97	Decreased by 45%	(436.0)	Decreased by 67%	(649.2)	Decreased by 78%	(755.8)
0.42-0.54	Decreased by 34%	(484.5)	Decreased by 62%	(883.5)	Decreased by 79%	(1125.8)
0.34-0.42	Increased by 62%	(530.1)	Increases by 71%	(607.0)	Increases by 74%	(632.7)
0.29-0.34	Increased by 35%	(319.2)	Increased by 42%	(383.0)	Increased by 67%	(611.0)
0.24-0.29	Increased by 51%	(290.7)	Increased by 64%	(364.8)	Increased by 72%	(410.4)
0.16-0.24	Increased by 35%	(79.80)	Increased by 38 %	(86.64)	Increased by 42%	(95.7)
0.08-0.16	Increased by 21%	(59.85)	Increased by 29%	(82.65)	Increased by 44%	(125.4)
0-0.08	Increased by 12%	(18.43)	Increased by 61%	(29.08)	Increased by 86%	(54.71)
-1-0	Increased by 16%	(21.02)	Increased by 57%	(33.80)	Increased by 66%	(55.76)

5. Outlook

We applied freely available Landsat imageries to study short-term landscape dynamics in the mine-reclaimed Kirchheller Heide, and identified two potential subsidence spots that are under risk of collapse and overall degradation and damage of vegetation (Figure 5). Thus, our results inform environmental management and mining reclamation experts about land surface and vegetation loss as a result of subsidence. Environmental management authorities in Kirchheller Heide should prioritise the indicated subsidence areas for further surface and subsurface investigation as well as for remediation and mitigation. The potential biodiversity and ecosystem impacts of subsidence should also be investigated.

In general, our study proves the virtue of RS and GIS for monitoring short-term geological changes and thus for predicting long term environmental impacts in reclaimed mine areas. In turn, we urge the importance of including RS and GIS monitoring in environmental conservation and management projects in addition to field monitoring [1-3]. Our approach is also useful for identifying ecological stress, surface erosion and inundation, and thus may provide important metrics for ecological restoration and infrastructure provision [2-4].

Our study also emphasises the need for proper backfilling and management of reclaimed mine areas [1-3]. Environmental regulations mostly address the direct impacts of mining activities and insufficiently address the long-term impacts of post-mining activities [2-4]. We recommend that environmental management should take advantage of satellite imageries and RS/GIS techniques [7]. The reclaimed mine areas should be regularly monitored for the identification of subsidence and surface collapses.

Field observatory and survey data should complement the applied RS techniques with freely available satellite data to validate our results [2]. Future studies should apply higher spatial resolution (e.g. 5m) satellite imageries, e.g. Quickbird and LIDAR images, for the identification of subsidence extent and magnitude in reclaimed mine areas [3,4]. RS based monitoring could also result in surface metrics for quantification of geological changes in reclaimed mine areas.

High and hyper spectral and temporal satellite imageries may provide landscape dynamics with higher precision than in our study [61-63]. For example, a comprehensive monthly variation analysis would provide a more precise information on the emergence and dynamics of subsidence zones, and images with higher coverage of bands would better identify subsidence spots that are not observed through the growth of waterbodies [61-63]. Future versions of this study should consider the use of these images for better informing environmental management and mining reclamation experts.

Acknowledgments:

The research was conducted as part of Rajchandar Padmanaban studies in the Ph.D. programme in Information Management at NOVA IMS, Universidade Nova de Lisboa.

Author Contributions: R.P. and P.C. have conceived the study. R.P. conducted image processing, classification accuracy assessment and indices calculation under the supervision of A.K.B. and P.C. R.P. and A.K.B. wrote the paper, P.C. revised the paper.

Conflicts of Interest: The authors declare no conflict of interest.

References

1. Brunn, A.; Dittmann, C.; Fischer, C.; Richter, R. Atmospheric correction of 2000 HyMAP data in the framework of the EU-project MINEO. In *Proceedings of SPIE*; 2001; Vol. Volume 454, pp. 382–392.

2. Dittmann, C.; Vosen, P.; Brunn, A. *MINEO (Central Europe) environment test site in Germany - Contamination/impact mapping and modelling - Final report*; 2002.

3. Eikhoff, J. Developments in the German coal mining industry. *Entwicklungen im Deutsch. Steinkohlenbergbau* 2007, *143*, 10–16+4.

4. Brunn, A.; Busch, W.; Dittmann, C.; Fischer, C.; Vosen, P. Monitoring Mining Induced Plant Alteration and Change Detection in a German Coal Mining Area using Airborne Hyperspectral Imagery. 2002.

5. Prakash, A.; Gupta, R. P. Land-use mapping and change detection in a coal mining area - a case study in the Jharia coalfield, India. *Int. J. Remote Sens.* 1998, *19*, 391–410.

6. Wang, C. C.; Lv, Y.; Song, Y. Researches on mining subsidence disaster management GIS's system. In *2012 International Conference on Systems and Informatics, ICSAI 2012*; 2012; pp. 2493–2496.

7. Song, J.; Han, C.; Li, P.; Zhang, J.; Liu, D.; Jiang, M.; Zheng, L.; Zhang, J.; Song, J. Quantitative prediction of mining subsidence and its impact on the environment. *Int. J. Min. Sci. Technol.* 2012, *22*, 69–73.

8. Morfeld, P.; Ambrosy, J.; Bengtsson, U.; Bicker, H.; Kalkowsky, B.; Ksters, A.; Lenaerts, H.; Ruther, M.; Vautrin, H. J.; Piekarski, C. The risk of developing coal workers' pneumoconiosis in german coal mining under modern mining conditions. *Ann. Occup. Hyg.* 2002, *46*, 251–253.

9. Carnec, C.; Delacourt, C. Three years of mining subsidence monitored by SAR interferometry, near Gardanne, France. In *European Space Agency, (Special Publication) ESA SP*; 2000; pp. 141–149.

10. Allgaier, F. K. Surface Subsidence over Longwall Panels in the Western United States. In *State of the Art of Ground Control in Longwall Mining and Mining Subsidence*; 1982; pp. 199–209.

11. Scott, M. J.; Statham, I. Development advice maps: mining subsidence. *Geol. Soc. London, Eng. Geol. Spec. Publ.* 1998, *15*, 391–400.

12. Hu, Z.; Hu, F.; Li, J.; Li, H. Impact of coal mining subsidence on farmland in eastern China. *Int. J. Surf. Mining, Reclam. Environ.* 1997, *11*, 91–94.

13. Zuo, C.; Ma, F.; Hou, J. Representatives of mining subsidence analysis visualization of China. *Liaoning Gongcheng Jishu Daxue Xuebao (Ziran Kexue Ban)/Journal Liaoning Tech. Univ. (Natural Sci. Ed.* 2014, *33*, 788–792.

14. Jat, M. K.; Garg, P. K.; Khare, D. Monitoring and modelling of urban sprawl using remote sensing and GIS techniques. *Int. J. Appl. Earth Obs. Geoinf.* 2008, *10*, 26–43.

15. Rajchandar, P.; Bhowmik, A. K.; Cabral, P.; Zamyatin, A.; Almegdadi, O.; Wang, S. Modelling Urban Sprawl Using Remotely Sensed Data: A Case Study of Chennai City, Tamilnadu. *entropy* 2017, *19*, 163.

16. Deck, O.; Verdel, T.; Salmon, R. Vulnerability assessment of mining subsidence hazards. *Risk Anal.* 2009, *29*, 1381–1394.

17. Venkatesan G; Padmanaban, R. Possibility Studies and Parameter Finding for Interlinking of Thamirabarani and Vaigai Rivers in Tamil Nadu, India. *Int. J. Adv. Earth Sci. Eng.* 2012, *1*, 16–26.

18. Monishiya, B. G.; Padmanaban, R. Mapping and change detection analysis of marine resources in Tuicorin and Vembar group of Islands using remote sensing. *Int. J. Adv. For. Sci. Manag.* 2012, *1*, 1–16.

19. Baek, J.; Kim, S.; Park, H.; Kim, K. Analysis of ground subsidence in coal mining area using SAR interferometry. 2008, *12*, 277–284.

20. Whittaker, B. N.; Reddish, D. J. Mining Subsidence in Longwall Mining with Special Reference to the Prediction of Surface Strains. In *Stability in Underground Mining II*; 1984.

21. Kuosmanen, V.; Laitinen, J.; Arkimaa, H. A comparison of hyperspectral airborne HyMap and spaceborne Hyperion data as tools for studying the environmental impact of talc mining in Lahnaslampi, NE.*New Qual. Environ. …* 2005.

22. S, S. L.; Padmanaban, R.; Thomas, V. Inventory of Liquefaction Area and Risk Assessment Region Using Remote Sensing. *Int. J. Adv. Remote Sens. GIS* 2013, *2*, 198–204.

23. Brunn, A.; Fischer, C.; Dittmann, C.; Richter, R. Quality Assessment, Atmospheric and Geometric Correction of airborne hyperspectral HyMap Data. *Geotech. Eng.* 2003, 13–16.

24. Lucas, R.; Ellison, J.; Mitchell, A.; Donnelly, B.; Finlayson, M.; Milne, A. Use of stereo aerial photography for quantifying changes in the extent and height of mangroves in tropical Australia. *Wetl. Ecol. Manag.* 2002.

25. Ferdinent, J.; Padmanaban, R. Development of a Methodology to Estimate Biomass from Tree Height Using Airborne Digital Image. *Int. J. Adv. Remote Sens. GIS* 2013, *2*, 49–58.

26. Padmanaban, R. Modelling the Transformation of Land use and Monitoring and Mapping of Environmental Impact with the help of Remote Sensing and GIS. *Int. J. Adv. Altern. Energy, Environ. Ecol.* 2012, *1*, 36–38.

27. Visalatchi; Padmanaban, R. Land Use and Land Cover Mapping and Shore Line Changes Studies in Tuticorin Coastal Area Using Remote Sensing. *Int. J. Remote Sens.* 2012, *1*, 1–12.

28. Padmanaban, R.; Sudalaimuthu, K. Marine Fishery Information System and Aquaculture Site Selection Using Remote Sensing and GIS. *Int. J. Adv. Remote Sens. GIS* 2012, *1*, pp 20-33.

29. Padmanaban, R. Integrating of Urban Growth Modelling and Utility Management System using Spatio Temporal Data Mining. *Int. J. Adv. Earth Sci. Eng.* 2012, *1*, 13–15.

30. Padmanaban, R.; Kumar, R. Mapping and Analysis of Marine Pollution in Tuticorin Coastal Area Using Remote Sensing and GIS. *Int. J. Adv. Remote Sens. GIS* 2012, *1*, 34–48.

31. Hinz, C. Wetter dienst http://www.wetterdienst.de/Deutschlandwetter.

32. Pebesma, E.; Bivand, R. S. S Classes and Methods for Spatial Data: the sp Package. *Econ. Geogr.* 2005, *50*, 1–21.

33. Pebesma, E.; Bivand, R.; Rowlingson, B.; Gomez-Rubio, V. Classes and Methods for Spatial Data. *URL http//CRAN. R-project. org/package= sp, R Packag. version* 2013.

34. Steve Morris; James Tuttle; Jefferson Essic. A Partnership Framework for Geospatial Data Preservation in North Carolina. *Libr. Trends* 2009, *57*, 516–540.

35. Hijmans, R. J.; Etten, J. van; Mattiuzzi, M.; Sumner, M.; Greenberg, J. A.; Lamigueiro, O. P.; Bevan, A.; Racine, E. B.; Shortridge, A. Package "raster." *R* 2014, 1–27.

36. Hijmans, R. J.; Etten, J. raster: Geographic analysis and modeling with raster data. *R Packag. version 2.4-20. http//CRAN.R-project.org/package=raster* 2012.

37. Vincenzi, S.; Zucchetta, M.; Franzoi, P.; Pellizzato, M.; Pranovi, F.; De Leo, G. A.; Torricelli, P. Application of a Random Forest algorithm to predict spatial distribution of the potential yield of Ruditapes philippinarum in the Venice lagoon, Italy. *Ecol. Modell.* 2011, *222*, 1471–1478.

38. Liaw,a; Wiener, M. Classification and Regression by randomForest. *R news* 2002, *2*, 18–22.

39. Breiman, L. Random forests. *Mach. Learn.* 2001, *45*, 5–32.

40. Chander, G.; Markham, B. L.; Helder, D. L. Summary of current radiometric calibration coefficients for Landsat MSS, TM, ETM+, and EO-1 ALI sensors. *Remote Sens. Environ.* 2009, *113*, 893–903.

41. Goslee, S. C. Analyzing Remote Sensing Data in R: The landsat Package. *J. Stat. Softw.* 2011, *43*.

42. Streiner, D. L. An introduction to multivariate statistics. *Can. J. Psychiatry* 1993, *38*, 9–13.

43. Bivand, R. S.; Pebesma, E. J.; Gómez-Rubio, V. *Applied Spatial Data Analysis with R*; 2008; Vol. 65.

44. Assal, T. J.; Anderson, P. J.; Sibold, J. Mapping forest functional type in a forest-shrubland ecotone using SPOT imagery and predictive habitat distribution modelling. *Remote Sens. Lett.* 2015, *6*, 755–764.

45. Walston, L. J.; Cantwell, B. L.; Krummel, J. R. Quantifying spatiotemporal changes in a sagebrush ecosystem in relation to energy development. *Ecography (Cop.).* 2009, *32*, 943–952.

46. Dubovyk, O.; Menz, G.; Conrad, C.; Kan, E.; Machwitz, M.; Khamzina, A. Spatio-temporal analyses of cropland degradation in the irrigated lowlands of Uzbekistan using remote-sensing and logistic regression modeling. *Environ. Monit. Assess.* 2013, *185*, 4775–4790.

47. Assal, T. J.; Anderson, P. J.; Sibold, J. Spatial and temporal trends of drought effects in a heterogeneous semi-arid forest ecosystem. *For. Ecol. Manage.* 2016, *365*, 137–151.

48. Masek, J. G.; Vermote, E. F.; Saleous, N. E.; Wolfe, R.; Hall, F. G.; Huemmrich, K. F.; Gao, F.; Kutler, J.; Lim, T. K. A landsat surface reflectance dataset for North America, 1990-2000. *IEEE Geosci. Remote Sens. Lett.* 2006, *3*, 68–72.

49. Assal, T. J.; Sibold, J.; Reich, R. Modeling a Historical Mountain Pine Beetle Outbreak Using Landsat MSS and Multiple Lines of Evidence. *Remote Sens. Environ.* 2014, *155*, 275–288.

50. Stehman, S. V Estimating the Kappa coefficient and its variance under stratified random sampling. *Photogramm. Eng. Remote Sens.* 1996, *62*, 401–407.

51. Halabisky, M.; Moskal, L. M.; Gillespie, A.; Hannam, M. Reconstructing semi-arid wetland surface water dynamics through spectral mixture analysis of a time series of Landsat satellite images (1984-2011). *Remote Sens. Environ.* 2016, *177*, 171–183.

52. Clough, B.F.; Ong, J.E.; Gong, W. K. Estimating leaf area index and photosynthetic production in canopies of the mangrove Rhizophora apiculata. *Mar. Ecol. Prog. Ser.* 1997, *159*, 285–292.

53. Chevrel, S.; Kopackova, V.; Fischer, C.; Ben Dor, E.; Adar, S.; Shkolnisky, Y.; Misurec, J. Mapping minerals, vegetation health and change detection over the sokolov lignite mine using multidate hyperspectral airborne imagery. In *EAGE/GRSG Remote Sensing Workshop*; 2012.

54. Green, E. P.; Mumby, P. J.; Edwards, A. J.; Clark, C. D.; Ellis, A. C. Estimating leaf area index of mangroves from satellite data. *Aquat. Bot.* 1997, *58*, 11–19.

55. Kovacs, J. M.; Wang, J.; Flores-Verdugo, F. Mapping mangrove leaf area index at the species level using IKONOS and LAI-2000 sensors for the Agua Brava Lagoon, Mexican Pacific. *Estuar. Coast. Shelf Sci.* 2005, *62*, 377–384.

56. Kovacs, J. M.; Flores-Verdugo, F.; Wang, J.; Aspden, L. P. Estimating leaf area index of a degraded mangrove forest using high spatial resolution satellite data. *Aquat. Bot.* 2004, *80*, 13–22.

57. Kovacs, J. M.; King, J. M. L.; Flores de Santiago, F.; Flores-Verdugo, F. Evaluating the condition of a mangrove forest of the Mexican Pacific based on an estimated leaf area index mapping approach. *Environ. Monit. Assess.* 2009, *157*, 137–149.

58. Bhowmik, A. K.; Cabral, P. Cyclone Sidr Impacts on the Sundarbans Floristic Diversity. *Earth Sci. Res.* 2013, *2*, 62–79.

59. Kovacs, J. M.; Wang, J.; Flores-Verdugo, F. Mapping mangrove leaf area index at the species level using IKONOS and LAI-2000 sensors for the Agua Brava Lagoon, Mexican Pacific. *Estuary. Coast. Shelf Sci.* 2005, *62*, 377–384.

60. Meza Diaz, B.; Blackburn, G. A. Remote sensing of mangrove biophysical properties: evidence from a laboratory simulation of the possible effects of background variation on spectral vegetation indices. *Int. J. Remote Sens.* 2003.

61. Brunn, Andreas.; Busch, W.; Dittmann, C.; Fischer, C.; and Vosen, P.; Monitoring mining induced plant alteration and change detection in a german coal mining area using airborne hyperspectral imagery. In *US Environ. Protection Agency Conf. on Remote Sensing of Vegetation*. 2003.

62. Millán, Virginia E.; García, Andreas Müterthies.; Kian Pakzad.; Sebastian Teuwsen.; Norbert Benecke.; Karsten Zimmermann.; Heinz-Jürgen Kateloe.; Axel Preuße.; Kristina Helle.; and Christian Knoth. GMES4Mining: GMES-based Geoservices for Mining to Support Prospection and Exploration and the Integrated Monitoring for Environmental Protection and Operational Security. *BHM Berg-und Hüttenmännische Monatshefte*. 2014, 66-73.

63. Brunn, Andreas.; Christoph Dittmann.; Christian Fischer.; and Rudolf Richter. Atmospheric Correction of 2000 HyMap TM Data in the Framework of the EU-Project Mineo. 2001.